The Working Cycle of a Resonant MEMS Heat Engine

H. Bardaweel[1], R. Richards[1], M. Anderson[2], C. Richards[1]
[1] School of Mechanical and Material Engineering
Washington State University Pullman, WA, USA, cill@wsu.edu
[2] Dept. of Mechanical Engineering
University of Idaho

Abstract: The working cycle of a dynamic MEMS heat engine is presented. Measurements of pressure and volume are acquired during engine operation and are used to construct pressure-volume diagrams for the engine cycle. A lumped parameter model of the engine is used to identify deviations from ideal behavior and the limits of the cycle. Experiments and theory indicate that the cycle for the resonant MEMS heat engine consists of constant-volume heat addition/rejection, and isothermal expansion/compression.

Key words: MEMS heat engine, micro heat engine, working cycle.

1. INTRODUCTION

Considerable effort has been put forth by several groups to produce MEMS dynamic heat engines based on rotating micromachinery that employ Otto, Brayton and Rankine cycles [1-4]. Our group has worked to develop a unique microscale dynamic heat engine based on a single flexible membrane that acts as both compressor and expander [5]. The engine, an external combustion device, consists of a cavity filled with a two-phase working fluid (PF5060) separated by two micro-machined square membranes. The engine is made up of three major components; a thermal switch to control heat addition and rejection, an evaporator, and an expander which produces mechanical work. In previous work we have shown the engine produces net mechanical power when operated at low frequency from a constant heat source at 60 C^o [6]. The engine has also been successfully integrated with a Swiss roll micro combustor to produce power [7].

In this study we characterize for the first time the working cycle of the engine using both experiments and modeling.

2. APPROACH

We have developed and validated a lumped parameter model which captures the basic physics associated with both the thermal and dynamic processes in the engine [8]. Experimentally the deflections of both the top and bottom membranes are used to infer the engine volume and pressure. Pressure volume diagrams are constructed to characterize the working cycle of the engine.

2.1 Experiment

The micro engine, shown in Fig. 1, consists of a cavity filled with a two-phase fluid bounded by top and bottom membranes. The flexible top membrane acts as an expander. Mechanical power is produced as the top membrane alternately expands and compresses the working fluid. The rigid bottom membrane acts as an evaporator. A capillary wick fabricated on the bottom membrane controls the layer of liquid-phase working fluid on the evaporator. A thermal switch (not shown) is used to control the timing and duration of the heat addition and heat rejection. Details on the fabrication, assembly, and operation are provided in [6 – 8].

The deflections of both the top and bottom membranes are measured with a laser vibrometer for a given periodic heat input. Engine volume is derived from the top membrane deflection, and engine pressure is derived from the bottom membrane deflection.

A linear transfer function analysis is used to interpret the data collected from the experiment. The heat rate $q(t)$ delivered to the engine is the input and the velocity of the upper membrane $u(t)$ is the output.

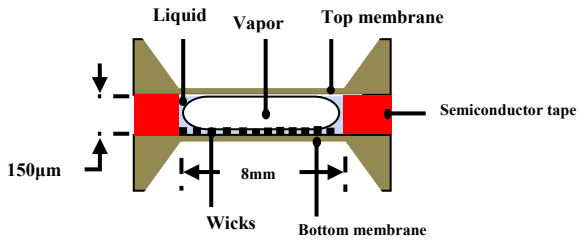

Fig.1: Schematic of engine.

2.2 Model

A lumped-parameter mathematical model of the engine was developed in previous work [9]. The expander/compressor is modeled as a moveable rigid diaphragm constrained by a spring of stiffness s and two dampers with coefficients b_f and b respectively. A moveable rigid evaporator provides the lower boundary. The motion of the upper diaphragm and evaporator are measured by the displacements x and x_h respectively. The engine is powered by a periodic alternating heat flux $q(t)$ applied to the evaporator component. The cavity is of diameter $2r_o$, and contains a saturated-vapor bubble of diameter $2r_i$ and liquid in the annulus.

The lumped-parameter mathematical model of the engine was developed by applying conservation laws to the vapor bubble and liquid film above the evaporator, and Newton's laws for the motion of the upper diaphragm and evaporator. The model was then linearized for analysis of engine performance. The linear model takes the form

$$\Delta \dot{V}_g + \left[\frac{(\pi r_i^2)^2}{s_h} + \frac{V_o}{\rho_o R T_o}\right]\Delta\dot{p} - \frac{V_o}{T_o}\Delta\dot{T} = \frac{BS}{\rho_o}\Delta T_l - \frac{S}{\rho_o}\sqrt{\frac{M}{2\pi R_u}}\frac{1}{\sqrt{T_o}}\left[\Delta p - \frac{\rho_o R}{2}\Delta T\right], \quad (1)$$

$$\frac{V_o}{T_o}\Delta\dot{T} - \frac{V_o}{\rho_o c_p T_o}\Delta\dot{p} = -\frac{h_B}{\rho_o c_p T_o}\Delta T, \quad (2)$$

$$\frac{(m+\bar{m})}{(\pi r_o^2)^2}\Delta\ddot{V}_g + \frac{(b_f+b)}{(\pi r_o^2)^2}\Delta\dot{V}_g + \frac{s}{(\pi r_o^2)^2}\Delta V_g = \Delta p, \quad (3)$$

$$\frac{C_T}{\rho_o h_{fg}}\Delta\dot{T}_l = \frac{q(t)}{\rho_o h_{fg}} - \frac{U}{\rho_o h_{fg}}\Delta T_l - \frac{B}{\rho_o}\Delta T_l + \frac{S}{\rho_o}\sqrt{\frac{M}{2\pi R_u}}\frac{1}{\sqrt{T_o}}\left[\Delta p - \frac{\rho_o R}{2}\Delta T\right]. \quad (4)$$

where $\Delta V_g = \pi r_o^2 x$ is the volume change of the vapor bubble caused by motion of the upper membrane; Δp, ΔT, and ΔT_l are the departures of vapor pressure, temperature, and liquid temperature from their ambient values. The coefficient B is given by

$$B = \frac{\partial}{\partial \Delta T_l}\left[\frac{p_l(T_o+\Delta T_l)}{\sqrt{T_o+\Delta T_l}}\right]_{\Delta T_l=0} = \frac{10^{\hat{A}-\frac{\hat{B}}{T_o+\hat{C}}}}{\sqrt{T_o}}\left[\frac{\hat{B}\ln 10}{(T_o+\hat{C})^2} - \frac{1}{2T_o}\right], \quad (5)$$

where $\hat{A}$, $\hat{B}$ and $\hat{C}$ are coefficients particular to the working fluid. Details of the model development and validation are provided in [9].

3. RESULTS

A schematic of the working cycle of the engine is illustrated in Fig. 2. The cycle consists of four processes; first heat is added to the evaporator membrane; second, working fluid is evaporated and the expander membrane is deflected upwards by the expansion of the fluid volume; third, heat is rejected via the thermal switch, and fourth, working fluid is condensed and the expander membrane deflects down compressing the working fluid.

An engine with a 10 mm expander side length, an 8 mm evaporator side length, and a cavity thickness of 150 μm was assembled. A periodic heat input of 1mJ with a 1% duty cycle was supplied to the engine at a frequency of 130 Hz. This frequency results in resonant operation.

The determination of the pressure and volume changes inside the engine is crucial in order to obtain the working cycle of the engine. Because the pressure and volume measurements are decoupled during resonance operation, the pressure and volume changes are determined independently for a resonance operation. This is done by evaluating the pressure and volume changes inside the engine using deflection of the bottom and top membranes respectively. The pressure changes are related to the deflection of the lower membrane through a calibrated pressure deflection curve. The volume under the expander

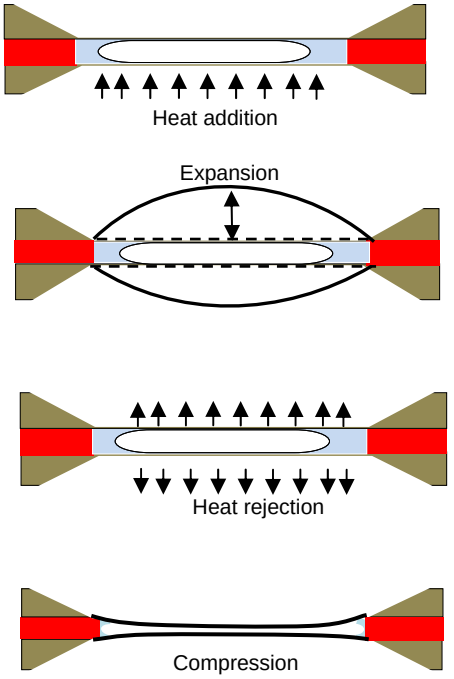

Fig. 2: Working cycle of micro heat engine.

membrane is determined by performing a double integral on the membrane deflection profile.

An experimental pressure-volume diagram for the engine is shown in Fig 3. At resonance, the pressure and volume in the engine cavity cyclically rise and fall 90 degrees out of phase. The engine cycle describes a closed loop. The points corresponding to heat addition and heat rejection are shown on the diagram.

The model PV diagram is obtained by solving the linear system and determining the state variables corresponding to volume and pressure. The corresponding prediction of the pressure-volume diagram is shown in Fig. 4. In both experimental and modeled results, the heat addition processes extend over only 1% of the cycle (1% duty cycle). Previously work has shown that short duration heat addition/rejection processes are desirable [8].

Some of the deviation between the model prediction and experimental pressure-volume relation may be attributed to the characteristics of the heat addition and rejection. In the model the heat addition is assumed to be a square pulse. However, in the experiment, the heat pulse is smeared out, due to the thermal capacitance of the evaporator membrane. Modifying the heat addition and rejection processes in the model from square wave processes to Gaussian processes, results in the predicted Pressure-Volume diagram shown in Fig. 5. This results in better agreement between the model and experiment.

Short time heat addition and heat rejection processes will, in the limit of zero time, approach constant volume processes. The expansion and compression processes, occurring with phase change, approximate isothermal processes. Thus, the cycle appears to consist of two isochoric processes and two isothermal processes.

4. CONCLUSIONS

The working cycle of a dynamic MEMS heat engine operating at resonance was obtained experimentally. Pressure-volume diagrams were constructed from experimental measurements of the deflection of the evaporator and expander membranes respectively. The P-V digrams show that the engine produces a working cycle. A lumped parameter model of the engine was used to predict the pressure – volume relation for an engine identical to the one used in the experiments. The correspondence between the model prediction and the experiment depends upon the shape of the heat input pulse used by the model. A Gaussian heat pulse shape resulted in better agreement than a square pulse. Modeling and experiment have shown that rapid heat addition and rejection leads to better performance. Fast heat transfer processes will, in the limit of zero time, approach constant volume processes. The expansion and compression processes, occurring with phase change, approximate isothermal processes. Thus, the idealized cycle appears to consist of two isochoric processes and two isothermal processes.

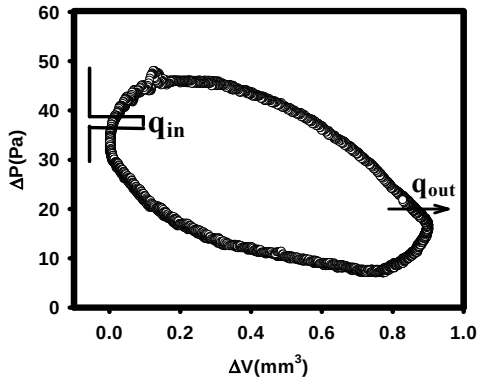

Fig.3: Measured P-V diagram for resonant engine.

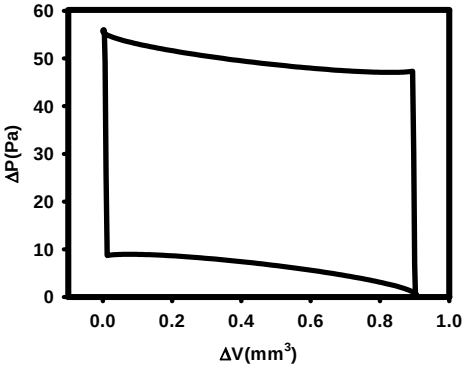

Fig. 4: Modeled P-V diagram for resonant engine.

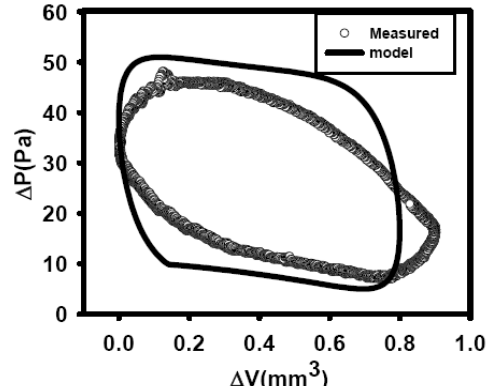

Fig. 5: Comparison of modeled and measured P-V diagram.

REFERENCES

1. Epstein A 2006 Millimeter-scale, MEMS gas turbine engines *ASME J. Eng. Gas Turbines Power* **126** 205-26
2. Fu K, Knobloch A, Martines C F, Walther D C, Fernandez-Pello C, Pisano P A and Liepmann D 2001 Design and fabrication of a silicon-based MEMS rotary engine *Proc. ASME Int Mech. Eng, Congress and Expo. (New York, 11-16 Nov)*
3. Frechette L, Lee C, Arslan S 2004 Development of a MEMS-based Rankine cycle turbine for power generation: Project status *Proc. PowerMEMS 04, 4th Workshop on Micro and Nano Technology for Power Gene and Energy Conv. Apps. (Kyoto, Japan, 28-30 Nov)*
4. Isomura K, Murayama M, Teramoto S, Hikichi K, Endo Y, Togo S and Tanaka S 2006 J. *Micromech. Microeng*. **16** S254-61.
5. Whalen S, Thompson M, Bahr D, Richards C and Richards R 2003 Design, fabrication and testing of P^3 micro heat engine *Sensors Actuators A Physical* **104** 290-8.
6. Cho J, Weiss L, Bahr D, Richards C and Richards R 2007 Power production by a dynamic micro heat engine with an integrated thermal switch *J. Micromech. Microeng.* **17** S217-23.
7. Cho J, Lee J, Lin C S, Sanford L N, Huang S J, Richards C D, Richards R F and Ahn J 2007 Fall Meeting of the Western States Section of the Combustion Institute Sandia National Laboratories, (Livermore, CA, 16 – 17 Oct)
8. Bardaweel H, Anderson M, Richards R and Richards C 2007 *Proc. PowerMEMS 07, 7th Workshop on Micro and Nano Technology for Power Gene and Energy Conv. Apps. (Freiberg, Germany, 29-30 Nov)*
9. Bardaweel H, Anderson M, Richards R and Richards C 2008 Optimization of dynamic and thermal performance of a resonant micro heat engine *J. Micromech. Microeng.* (accepted)